Arch. Metall. Mater. **63** (2018), 4, 1701-1708

DOI: 10.24425/amm.2018.125095

B. ZHOU*,***, CH. ZHU*, G. LI*#, Z. LUO**, Y. GAO**, S. BAO*, J. SCHNEIDER****

EFFECT OF SULFUR AND ACID SOLUBLE ALUMINUM CONTENT ON PRECIPITATE AND MICROSTRUCTURE OF GRAIN-ORIENTED SILICON STEEL

The combined effect of sulfur (S) and acid soluble aluminum (Al_s) content on precipitates and microstructures in grain-oriented silicon steel were investigated. The results show that there are dominant AlN and a little amount of MnS-AlN composite in annealed hot-rolled band, and the amount of precipitates increases distinctly with increasing Al_s content, while S content plays a negligible role. The inhibitors that precipitate during hot band annealing can restrain the grain growth during hot band annealing and primary annealing, and the smaller grains of annealed hot-rolled band can contribute to the formation of {111} <112> texture during primary annealing. Lower S content is conducive to the formation of {111} <112> texture during primary annealing by promoting the formation of Goss texture during hot rolling.

Keywords: grain-oriented silicon steel; sulfur; acid soluble aluminum; precipitate; microstructure and texture

1. Introduction

Grain-oriented silicon steel is an important soft magnetic material which is widely used as the core material in electrical transformers because of extremely high magnetic induction and low core loss along the rolling direction [1-3]. A key requirement for producing this steel is to obtain sharp {110} <001> texture (Goss texture) component by secondary recrystallization, which needs a complex processing scheme such as continuous casting, slab reheating, hot rolling, normalizing annealing, cold rolling, primary recrystallization annealing, secondary recrystallization annealing, heat flattening coating and so on. In order to obtain sharp Goss texture component after secondary recrystallization, the fine and dispersed precipitates which are used as "inhibitors" are indispensable [4-6]. Extensive studies have been done on the inhibitors and the results show that the inhibitors can restrain the normal grain growth during primary recrystallization annealing, thus promote the abnormal growth of Goss grains during secondary recrystallization [7-9]. In recent years, although many types of grain growth inhibitors such as AlN [2], MnS [8], MnSe [10], $Cu_{2-x}S$ [11] and Nb(C, N) [12], have now come into use for developing sharp Goss texture in grain-oriented silicon steel, most of the grain-oriented silicon steel is manufactured using MnS and AlN as the main inhibitors for promoting the magnetic property [13-16].

It has been accepted that MnS precipitates mainly during hot rolling because of the hot deformation [8,17], while the preparation of AlN is classified into two categories. One is the nitriding technology [13,14,16] where the steel is nitrided by the reaction between the sheet surface and the atmosphere during secondary recrystallization annealing, or nitrided with NH_3-containing atmosphere for short time after decarburization annealing. The other is the hot band annealing before cold rolling [18-20], in this way the hot-rolled band is often heated to a higher temperature for getting the γ phase to make AlN dissolve completely, and then the new nano-scale AlN can precipitate during the subsequent phase transformation of $\gamma \rightarrow \alpha$ in subsequent cooling and holding process. Both the AlN that precipitates during hot band annealing and nitriding process are well known that they can affect secondary recrystallization. Although, nitriding is now widely used for getting a large amount of AlN, it might not be omnipotent for controlling the secondary recrystallization [14]. In other words, hot band annealing is also necessary for producing grain-oriented silicon steel with lower slab heating temperature [21]. Our previous researches have shown that the MnS and AlN precipitates during hot rolling and hot band annealing, respectively, and can have a significant influence on the microstructure of hot-rolled band and annealed hot-rolled band by controlling the S and Al_s content [22,23]. In consideration of the structure memory during the production process, the MnS and AlN can also be thought to have a significant effect on the primary and secondary recrystallization, however, the effect of MnS and AlN are not studied to the best of our understanding.

* WUHAN UNIVERSITY OF SCIENCE AND TECHNOLOGY, STATE KEY LABORATORY OF REFRACTORIES AND METALLURGY, WUHAN, HUBEI, CHINA
** NATIONAL RESEARCH CENTER FOR SILICON STEEL, CHINA BAOWU STEEL GROUP CORPORATION LIMITED, WUHAN, HUBEI, CHINA
*** TECHNIQUE CENTER, LIUZHOU IRON&STEEL CO., LTD, LIUZHOU, GUANGXI, CHINA
**** TECHNISCHE UNIVERSITÄT BERGAKADEMIE FREIBERG, INSTITUTE OF METAL FORMING, FREIBERG, GERMANY

Corresponding author: liguangqiang@wust.edu.cn

The aim of present work was to investigate the combined impact of S and Al_s content on the primary and secondary recrystallization microstructure and texture of grain-oriented silicon steel with lower slab reheating temperature.

2. Experimental

Grain-oriented silicon steels containing different S content and Al_s content were prepared by a 100 kg vacuum induction furnace at 1640°C and were cast into 210 mm × 120 mm × (30-35) mm ingots. Then the steel samples were dissolved in HCl acid solution (1: 1 in volume with pure water) and the Al_s contents were determined by Inductively Coupled Plasma-Atomic Emission Spectrometry (ICP-AES), the C contents were determined by Infrared Carbon-Sulfur Determinator. The main chemical composition of the specimens is listed in Table 1. The ingots were reheated at 1250°C and hot rolled in three passes. The thickness of the ingots after finishing rolling at 970°C was 2.6 mm. After hot rolling, the specimens were treated by normalizing annealing in a tubular annealing furnace, as shown in Fig. 1. Then the specimens were cold rolled to 0.22 mm with a cold reduction of 91%. Following the cold rolling, the specimens were annealed at 830°C for 150 s in a wet atmosphere of 66.7% H_2 and 33.3% N_2 for decarburization and primary recrystallization. For the analysis about the microstructural evolution during primary recrystallization, the specimens were extracted at 20 s, 30 s, 40 s and 50 s during primary recrystallization annealing. The annealing separator which mainly consists of MgO was coated on the surface of primary annealed specimens. After that the specimens were heated up to 600°C and held for 2 h in order to remove the crystal water, then immediately heated to 1200°C with a heating rate of 17 K h^{-1} under a 75% H_2 and 25% N_2 atmosphere and maintained at 1200°C for 20 h under a 100% H_2 atmosphere for purification.

The precipitates in annealed hot-rolled bands were extracted by carbon extraction-replica technique and examined using a JEM-2100 transmission electron microscope (TEM).

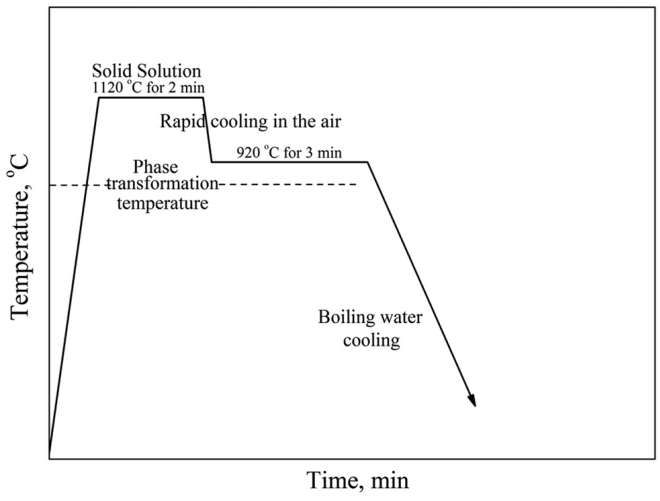

Fig. 1. Heat treatment pattern for hot band annealing

150 images in the fields of view were taken for each specimen and the number and size of the precipitates were measured by an Image-Pro Plus image analysis software. The microstructure and texture were determined by an optical microscope and an electron backscattered diffraction (EBSD) system equipped at a Nova 400 Nano field emission scanning electron microscope (FE-SEM). Optical microscopy and EBSD were applied on longitudinal sections as defined by the rolling direction (RD) and the normal direction (ND). The texture of secondary annealed band was measured at the surface using X-ray diffraction and the results were shown by complete {100} pole figures.

TABLE 1

Chemical composition of the tested steels (wt.%)

Sample	C	Si	Mn	Al_t	N	S	Al_s	Fe
1	0.047	3.03	0.11	0.014	0.0059	0.0037	0.010	Balance
2	0.049	3.16	0.10	0.018	0.0063	0.0068	0.015	Balance
3	0.053	3.20	0.10	0.027	0.0085	0.0071	0.025	Balance

3. Results

3.1. Precipitate and microstructure of annealed hot-rolled bands with different S content and Al_s content

Precipitate characterization was carried out using TEM combined with EDS analysis, as shown in Fig. 2. It should be noted that because nitrogen is a light element, the peaks of N in nano-scaled precipitates are difficult to be detected by EDS method. Meanwhile, the peaks of Ni can be observed because of the use of nickel mesh for getting the carbon film with precipitates on it. From Fig. 2 it can be found that the types of precipitates in these three tested steels are the same. One is AlN with irregular shape and smaller size; another is composite precipitate of MnS and AlN with ellipsoidal shape and significantly larger size. It also can be found that there are dominant AlN in the specimens and few composite precipitates can be observed. Clearer composition and morphology of the composite precipitate is shown in Fig. 3. It can be seen that MnS is nucleus of the composite precipitate and AlN precipitates on it.

Fig. 4 shows the number and size distribution of precipitates in the specimens with different S and Al_s content. It can be seen that a large number of precipitates can be obtained after hot band annealing. The amount is 1-2 order higher and the average size is several decades' nanometers smaller than that in hot-rolled band which has been studied in our previous research [22], which means that the hot band annealing is effective for obtaining more fine precipitates. From Fig. 4 it also can be found that the number of precipitates increases with the increasing Al_s content, while the average size doesn't change much and are in the range of 40 to 50 nm.

The microstructure of annealed hot-rolled band was determined by an optical microscope and the results are shown in Fig. 5. It can be seen that large inhomogeneity across the thickness exists in the specimen, and coarse grains in surface, small grains

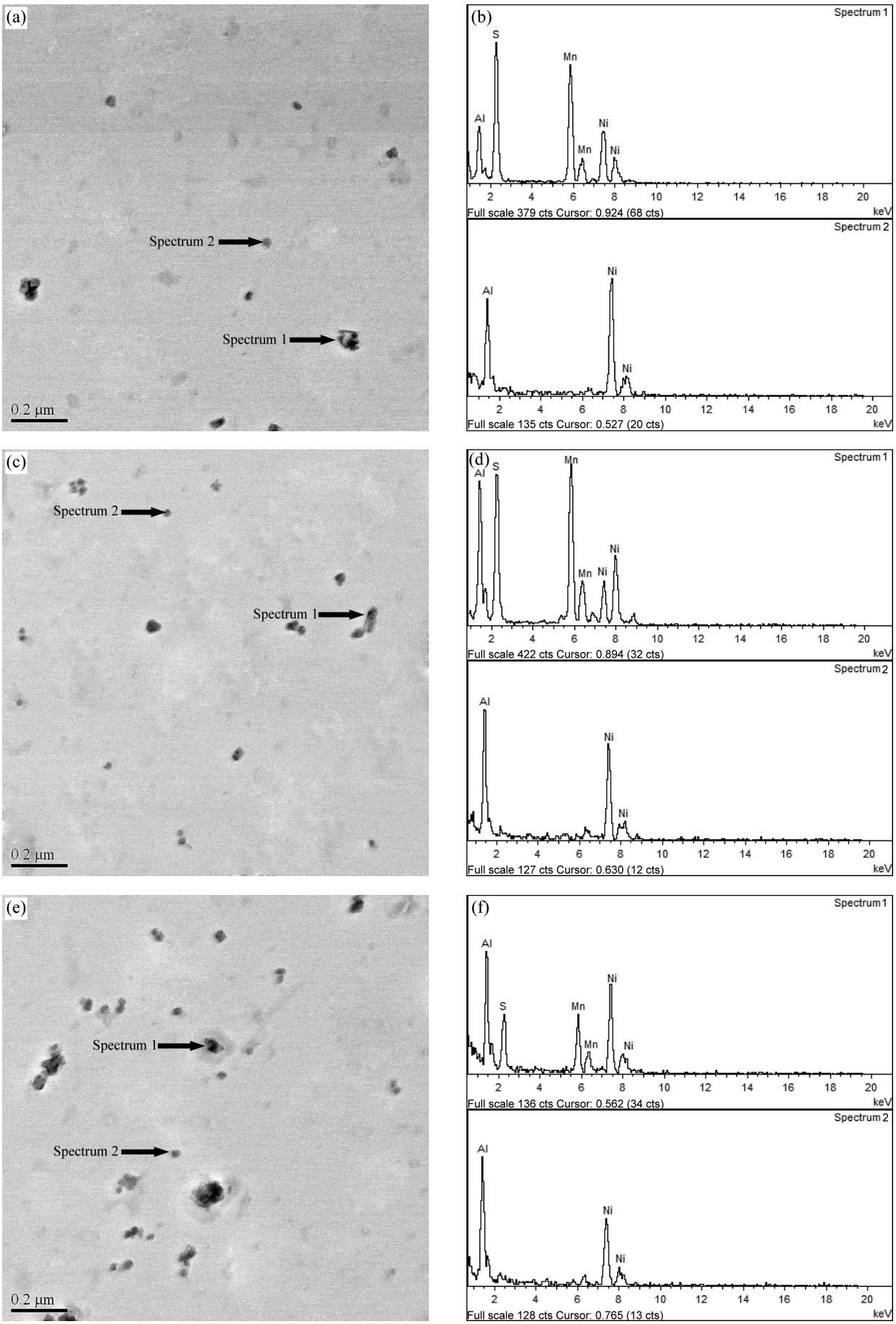

Fig. 2. TEM micrographs and EDS analyses of precipitates in annealed hot-rolled bands. (a) 0.0037 wt.% S and 0.010 wt.% Al_s; (b) 0.0068 wt.% S and 0.015 wt.% Al_s; (c) 0.0071 wt.% S and 0.025 wt.% Al_s

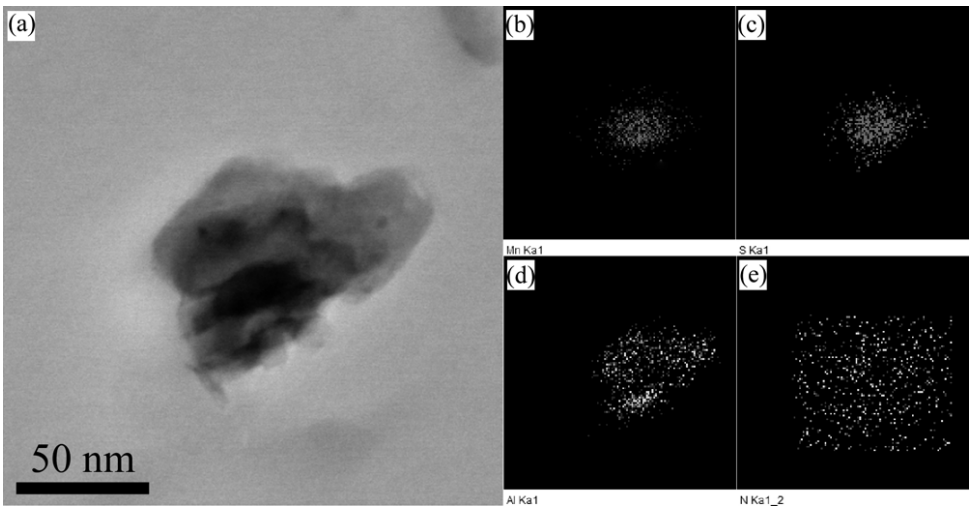

Fig. 3. Element mapping of the composite precipitate extracted from annealed hot-rolled bands

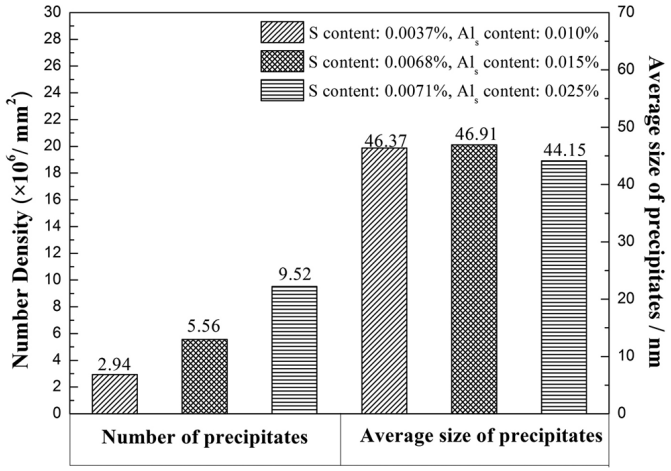

Fig. 4. Effect of S and Al_s content on number density and average size of precipitates in annealed hot-rolled bands

in subsurface and large elongated ferrite grains in center can be observed. In addition, an evident difference can be found between these three tested steels and the average grain size was measured along the thickness direction using a mean linear intercept method. The average grain size increases from 37.3 μm to 47.5 μm when the Al_s content decreases from 0.025 wt.% to 0.015 wt-%. In the specimen with 0.0037 wt.% S and 0.010 wt.% Al_s, the average grain size is 52.6 μm, which means that the grain size still increases with the decreasing Al_s content even though there is a decrease in S content.

3.2. Microstructures and textures of primary and secondary annealed bands with different S content and Al_s content

Fig. 6 illustrates the microstructures of specimens with different S and Al_s content during primary recrystallizaiton annealing at 830°C for different holding time. It can be seen that the degree of recrystallization increases and the amount of

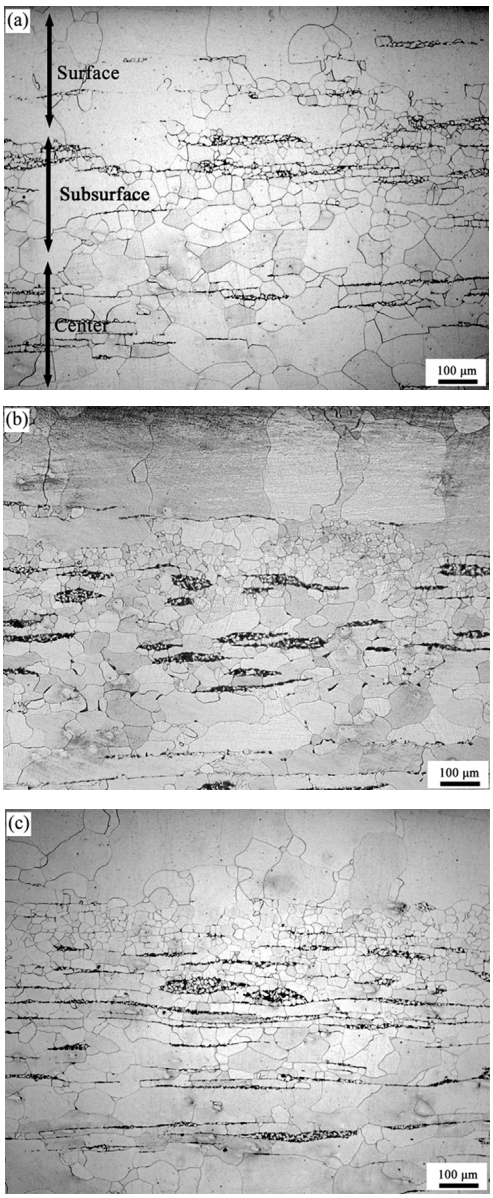

Fig. 5. The microstructures of annealed hot-rolled bands. (a) 0.0037 wt.% S and 0.010 wt.% Al_s; (b) 0.0068 wt.% S and 0.015 wt.% Al_s; (c) 0.0071 wt.% S and 0.025 wt.% Al_s

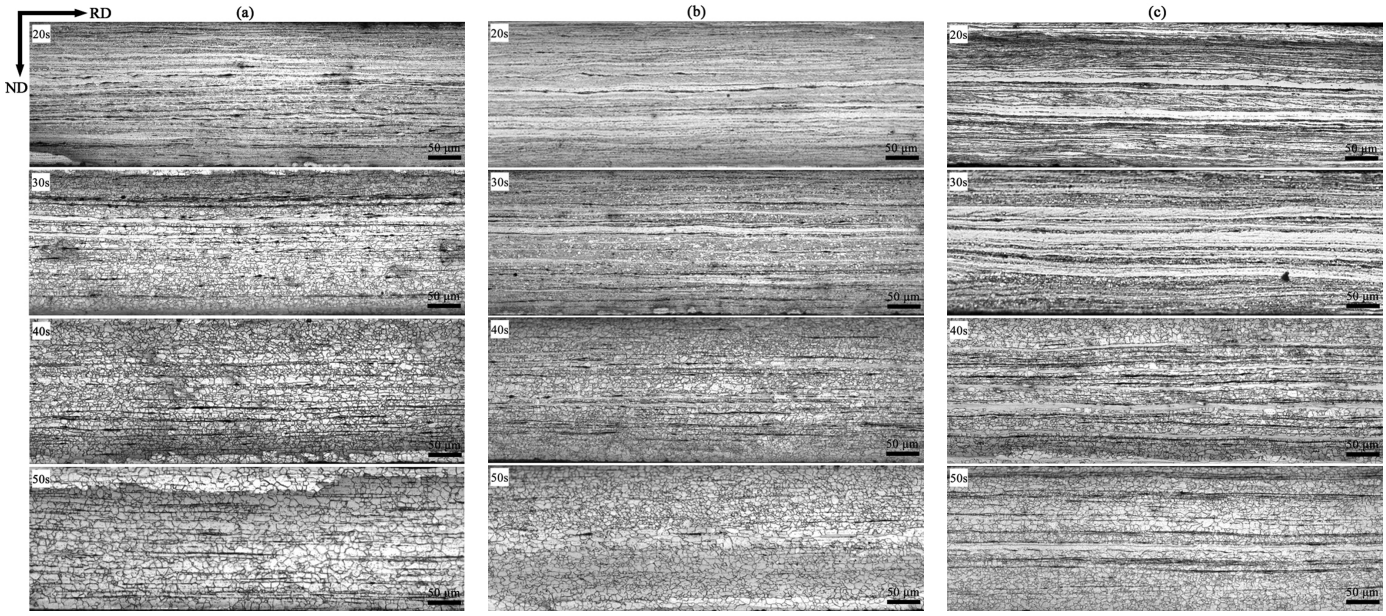

Fig. 6. The microstructural evolutions during primary recrystallizaiton annealing. (a) 0.0037 wt.% S and 0.010 wt.% Al_s; (b) 0.0068 wt.% S and 0.015 wt.% Al_s; (c) 0.0071 wt.% S and 0.025 wt.% Al_s

banding structures decreases with the increase of holding time. In the specimen with 0.0037 wt.% S and 0.010 wt.% Al_s, partial recrystallization occurred after holding for 20 s, and after holding for 40 s the specimen recrystallized completely and no banding structures can be observed. While no obvious recrystallization occurred after holding for 20 s in the specimen with 0.0068 wt.% S and 0.015 wt.% Al_s, and the recrystallized grains can be observed after holding for 30 s. The time for recrystallizing completely is 50 s, which is later than that in the specimen with 0.0037 wt.% S and 0.010 wt.% Al_s. In the specimen with 0.0071 wt.% S and 0.025 wt.% Al_s, some banding structures still existed after holding for 50 s, it is to say that this specimen need longest time to recrystallize completely.

After primary recrystallizaiton annealing, the microstructure and texture were studied by EBSD, as shown in Figs. 7-9. From Fig. 7a-c it can be found that a great difference presents in the microstructures of primary annealed bands with different S and Al_s content, and the grain size distribution is shown in Fig. 7d. It should be noted that the grains which are smaller than 5 μm are not included in the size distribution. It can be seen that the grains are in the size range of 5-45 μm, and approximately 90% of the grains are in the size range of 5-20 μm. The average size and standard deviation of the grains were obtained from the EBSD results, as shown in Fig. 7d. The most uniform and smallest grains can be observed in the specimen with highest Al_s content, and the grain size increases with the decrease of Al_s content.

The textures of completely primary recrystallization bands are shown in Fig. 8. It can be seen that texture types are similar to each other, and the texture is characterized by strong γ fiber with a peak at {111} <112> and the {411} <148> texture component is also included; while Goss texture component is very weak with an intensity lower than 1. However, an apparent difference of the texture intensities can be found between these three tested steels. The proportions and intensities of {111} <112> texture

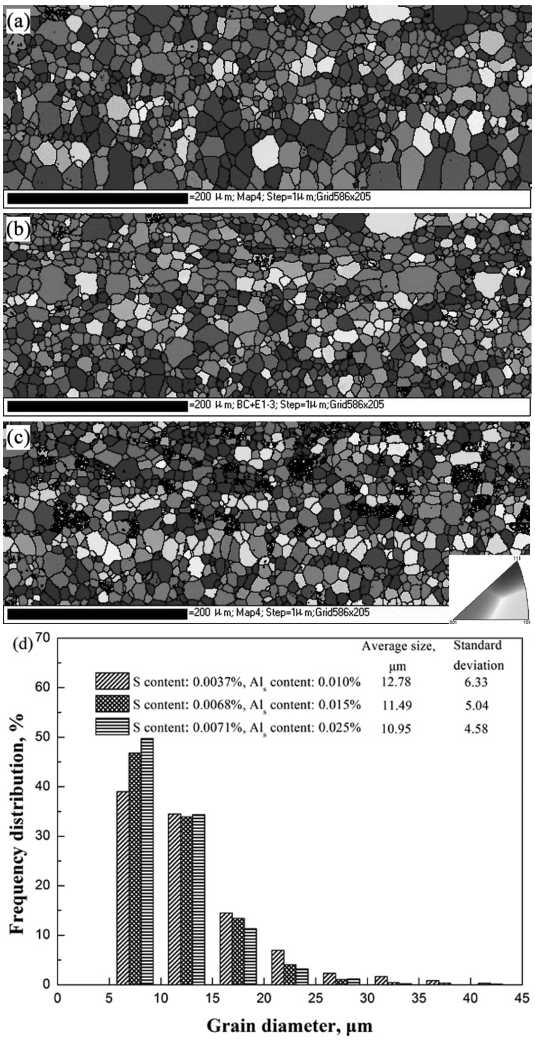

Fig. 7. The microstructures (a-c) and grain size distribution (d) of primary annealed bands. (a) 0.0037 wt.% S and 0.010 wt.% Al_s; (b) 0.0068 wt.% S and 0.015 wt.% Al_s; (c) 0.0071 wt-% S and 0.025 wt.% Al_s; (d) the grain size distribution

component in primary annealed bands were obtained from EBSD results, as shown in Fig. 9. Highest intensity and most amount of {111} <112> texture component can be observed in the specimen with 0.0071 wt.% S and 0.025 wt.% Al_s, while lower intensity and less amount of {111} <112> texture component is present in the specimen with 0.0068 wt.% S and 0.015 wt.% Al_s. With regard to the specimen with 0037 wt.% S and 0.010 wt.% Al_s, although the lowest Al_s content is present in it, higher intensity and more amount of {111} <112> texture component can be found in it when compared to the specimen with 0.0068 wt.% S and 0.015 wt.% Al_s.

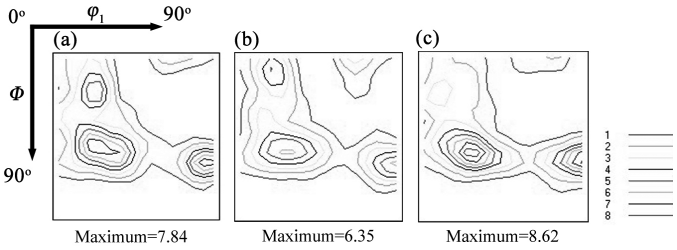

Fig. 8. ODFs sections of $\varphi_2 = 45°$ of primary annealed bands. (a) 0.0037 wt.% S and 0.010 wt.% Al_s; (b) 0.0068 wt.% S and 0.015 wt.% Al_s; (c) 0.0071 wt.% S and 0.025 wt.% Al_s

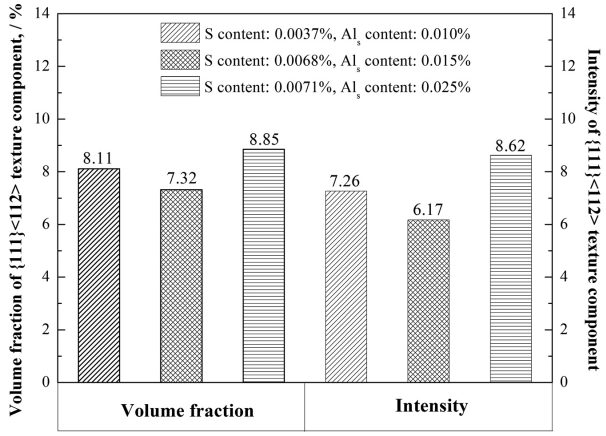

Fig. 9. Proportions and intensities of {111} <112> texture component in primary annealed bands with different S content and Al_s content

Fig. 10 shows the microstructures of secondary annealed bands with different S and Al_s content. It can be found that the microstructure is not a complete secondary recrystallized microstructure, a mixture of fine grains with a size smaller than 1 mm and large secondary recrystallized grains can be observed. Nevertheless, a big difference of the microstructures is present in these three tested steels. More complete secondary recrystallization is present in the specimen with 0.0071 wt.% S and 0.025 wt.% Al_s, while similar secondary recrystallized microstructure with lower degree of secondary recrystallization can be observed in the specimens with 0.015 wt.% Al_s and 0.010 wt.% Al_s. The secondary recrystallized texture is shown by the complete {100} pole, as shown in Fig. 11. From this figure it can be found that the specimen with 0.0071 wt.% S and 0.025 wt.% Al_s has the highest intensity of Goss texture component. While in the specimen with 0.0037 wt.% S and 0.010 wt.% Al_s and in the specimen with 0.0068 wt.% S and 0.015 wt.% Al_s, there are similarly weak Goss texture component.

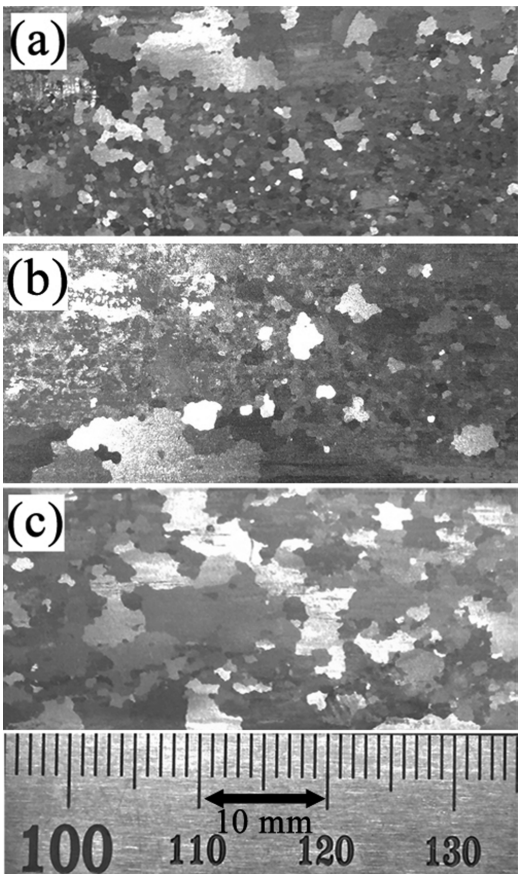

Fig. 10. The microstructures of secondary annealed bands. (a) 0.0037 wt.% S and 0.010 wt.% Al_s; (b) 0.0068 wt.% S and 0.015 wt.% Al_s; (c) 0.0071 wt.% S and 0.025 wt.% Al_s.

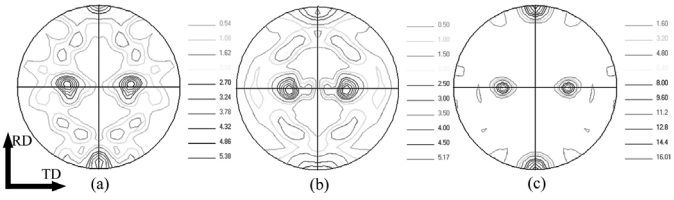

Fig. 11. (100) pole figures of secondary annealed bands. (a) 0.0037 wt.% S and 0.010 wt.% Al_s; (b) 0.0068 wt.% S and 0.015 wt.% Al_s; (c) 0.0071 wt.% S and 0.025 wt.% Al_s.

4. Discussion

4.1. The effect of S and Al_s content on the precipitation of inhibitors during hot band annealing

The AlN in grain-oriented silicon steel can be divided into three classes: the A type with a size smaller than 10 nm; the B type with a size between 20 and 50 nm; the C type with a size larger than 200 nm, and the more effective B type AlN was proved to precipitate mainly during hot band annealing [18], while the MnS was proved to precipitate mainly during hot rolling

[24,25]. According to the classical nucleation theory, AlN tends to precipitate on the pre-existing MnS due to lower free energy for precipitation, so not only AlN but the composite precipitate of MnS and AlN which form by using MnS as the nucleus can be observed in the annealed hot-rolled band. The MnS in hot-rolled bands with these compositions has been studied in our previous research [22] and the amount is 1-2 order lower than the precipitates in annealed hot-rolled band. Meanwhile, the coarsening of MnS during hot band annealing makes the size of most MnS-AlN composite larger than 100 nm, which results in that only few fine composites exist in the annealed hot-rolled band. So although the specimen with 0.0037 wt.% S and 0.010 wt.% Al_s has the most precipitates in hot-rolled band when compared to other two specimens [22], it has fewer precipitates in annealed hot-rolled band. It can be concluded that the effect of S content on the precipitation behavior of inhibitors during hot band annealing is inconspicuous. In our previous research the effect of Al_s content on AlN precipitation during hot band annealing has been studied and the volume fractions of AlN in these three tested steels can be obtained by theoretical calculation [23]. The results show that the volume fractions of AlN are 2.91×10^{-5}, 4.38×10^{-5} and 7.42×10^{-5}, respectively. That is why more fine precipitates can be observed in the specimen with higher Al_s content.

4.2. The effect of S and Al_s content on the microstructure and texture of primary and secondary annealed band

During primary recrystallization annealing, there are mainly recrystallization process of banding structure and grain growth of recrystallized grains. Many investigations on primary recrystallization annealing have been done and it was shown that the primary microstructure and texture depend sensitively on the precipitates, microstructure and texture in specimens prior to primary recrystallization annealing [26-29]. In present research, a large amount of precipitates was observed after hot band annealing, and these precipitates can have a great inhibition on the primary recrystallization by hindering the growth of subgrains, which can be explained by the following Eq. (1) [30,31].

$$P = P_D - P_Z = \frac{\alpha\gamma_s}{R} - 3f\frac{\gamma_s}{2r} \quad (1)$$

Where P is the driving force for subgrain growth; P_D is the driving force causing by interface energy of subgrain; P_Z is the Zener resistance causing by particles; α is a shape factor; R and r are the average radii of subgrain and particle, respectively; f is the volume fraction of particles; γ_s is the specific grain boundary energy. Which indicates that more fine precipitates can achieve a strong pinning force on recrystallization, that is why the specimen with more precipitates in it recrystallized later, as shown in Fig. 6. Meanwhile, more fine precipitates are accepted to have a stronger inhibiting effect on the grain growth [30,31]. Thus, more uniform and smaller grains can be observed in the specimen with higher Al_s content.

The large amount of inhibitors that precipitated during hot band annealing can also restrain the grain growth during hot band annealing. Hence, after hot band annealing the specimens have grains with different sizes in them and smaller average grain size is in the specimen with more precipitates, as shown in Fig. 5. Kumano's work [28, 29] has shown that the grain size of annealed hot-rolled band has a great effect on the primary texture, and the smaller grain can promote the formation of {111} <112> texture component in primary annealed band. So, when compared to the specimen with 0.0071 wt.% S and 0.025 wt.% Al_s, lower intensity and less amount of {111} <112> texture component is present in the specimen with 0.0068 wt.% S and 0.015 wt.% Al_s. Moreover, the Goss texture component in specimen before cold rolling can rotate to {111} <110> texture component during cold rolling with a high reduction, and then rotate to {111} <112> texture component during subsequent primary annealing [32]. It has been proved in our previous research [22] that significantly higher Goss texture component can be observed in the specimen with 0.0037 wt.% S and 0.010 wt.% Al_s. Thus, although the grains in annealed hot-rolled band with 0.0037 wt.% S and 0.010 wt.% Al_s are larger than that in specimen with 0.0068 wt.% S and 0.015 wt.% Al_s, higher intensity and more amount of {111} <112> texture component can be observed in it.

In the primary annealed band it also can be found that little Goss texture component existed, which can be explained by the extraordinarily high cold-rolled reduction used in our research, and that can be regarded as the reason for obtaining a mixture of fine grains and large secondary recrystallized grains after secondary annealing [33,34]. Besides the higher intensity and proportion of Goss texture component, the abundant and fine precipitates and the fine and homogeneous primary grains as well as the higher intensity and proportion of {111} <112> texture component are proved to be essential for the secondary recrystallization [26,35]. Thus, the specimen with 0.0071 wt.% S and 0.025 wt.% Al_s which has the most fine precipitates, the most homogeneous primary grains and the highest intensity and proportion of {111} <112> texture component can get the most complete secondary recrystallization microstructure and highest intensity of Goss texture after secondary annealing. Although, more fine precipitates and more homogeneous primary grains can be observed in the specimen with 0.0068 wt.% S and 0.015 wt.% Al_s when compared to the specimen with 0.0037 wt.% S and 0.010 wt.% Al_s, lower intensity and less amount of {111} <112> texture component is also observed, which may result in the similarly lower degree of secondary recrystallization and weaker Goss texture after secondary annealing.

5. Conclusions

The development of microstructure and texture in grain-oriented silicon steel with different S content and Al_s content was investigated. The results can be summarized as below:

(1) The precipitates in annealed hot-rolled band are dominant AlN and a little amount of MnS-AlN composite in which

MnS was the nucleus of AlN. The effect of S content on the precipitation of inhibitors during hot band annealing is negligible, while the amount of precipitates increases distinctly with increasing Al_s content.

(2) Fine precipitates can retard the recrystallization of banding structures and the growth of recrystallized grains during primary annealing, and more uniform and smaller grains can be obtained in the primary annealed specimen with higher Al_s content.

(3) Higher Al_s content is conducive to the formation of {111} <112> texture component in primary annealed band by the stronger pinning effect of more fine precipitates on grain growth during hot band annealing, and lower S content can also contribute to the formation of {111} <112> texture component by promoting the formation of Goss texture component during hot rolling.

(4) More complete secondary recrystallization microstructure and higher intensity of Goss texture in secondary annealed band are attributed to more fine precipitates, more homogeneous and smaller grains and higher intensity and proportion of {111} <112> texture component in primary annealed band.

Acknowledgement

This work was funded by the National Natural Science Foundation of China (No. 51104109, No. 51674180 and No.51274155). The authors of this paper thank the National Natural Science Foundation of China.

REFERENCES

[1] V. Stoyka, F. Kováč, O. Stupakov, I. Petryshynets, Mater. Charact. **61** (11), 1066-1073 (2010).

[2] T. Kubota, M. Fujikura, Y. Ushigami, J. Magn. Magn. Mater. **215-216**, 69-73 (2000).

[3] Z.S. Xia, Y.L. Kang, Q.L. Wang, J. Magn. Magn. Mater. **320** (23), 3229-3233 (2008).

[4] Y. Li, W.M. Mao, P. Yang, J. Mater. Sci. Technol. **27** (12), 1120-1124 (2011).

[5] G. Klaus, A. Giuseppe, F. Stefano, L. Guy, Steel Res. Int. **76** (6), 413-421 (2005).

[6] K. Jenkins, M. Lindenmo, J. Magn. Magn. Mater. **320** (20), 2423-2429 (2008).

[7] Y. Ushigami, T. Kubota, N. Takahashi, ISIJ Int. **38** (6), 553-558 (1998).

[8] T. Obara, H. Takeuchi, T. Takamiya, T. Kan, J. Mater. Eng. Perform. **2** (2), 205-210 (1993).

[9] M. Matsuo, ISIJ Int. **29** (10), 809-827 (1989).

[10] T. Takamiya, O. Furukimi, Tetsu-to-Hagané **100** (11), 1413-1420 (2014).

[11] T. Sakai, T. Shimazu, K. Chikuma, M. Tanino, M. Matsuo, Tetsu-to-Hagané **70** (15), 2049-2056 (1984).

[12] H. Klaus, V. Constantin, D. Ana, Steel Res. Int. **73** (10), 453-460 (2002).

[13] T. Kumano, T. Haratani, N. Fujii, ISIJ Int. **45** (1), 95-100 (2005).

[14] T. Kumano, Y. Ohata, N. Fujii, Y. Ushigami, T. Takeshita, J. Magn. Magn. Mater. **304** (2), 602-607 (2006).

[15] J. Harasea, R. Shimizub, J. Magn. Magn. Mater. **254-255** (1), 343-345 (2003).

[16] T. Kumano, T. Haratani, Y. Ushigami, ISIJ Int. **43** (3), 400-409 (2003).

[17] S. Mishra, V. Kumar, Mater. Sci. Eng. B-ADV **32** (3), 177-184 (1995).

[18] T. Sakai, M. Shiozaki, K. Takashina, J. Appl. Phys. **50** (B3), 2369-2371 (1979).

[19] C. Ling, L. Xiang, S.T. Qiu, Y. Gan, J. Iron Steel Res. Int. **21** (7), 690-694 (2014).

[20] H. Li, Y.L. Feng, M. Song, J.L. Liang, D.Q. Cang, T. Nonferr. Metal. Soc. **24** (3), 770-776 (2014).

[21] M.C. Tsai, Y.S. Hwang, J. Magn. Magn. Mater. **322** (18), 2690-2695 (2010).

[22] B.W. Zhou, C.Y. Zhu, G.Q. Li, Y. Fu, Mater. Sci. Tech-Lond. **31** (15), 1809-1817 (2015).

[23] B.W. Zhou, C.Y. Zhu, G.Q. Li, X.L. Wan, J. Schneider, Steel Res. Int. **87** (12), 1702-1714 (2016).

[24] W.M. Mao, Front. Mater. Sci. China **2** (3), 233-238 (2008).

[25] T. Takamiya, T. Obara, M. Muraki, M. Komatsubara, Tetsu-to-Hagané **89** (5), 518-523 (2003).

[26] Y. Wang, Y.B. Xu, Y.X. Zhang, F. Fang, X. Lu, R.D.X. Misra, G.D. Wang, Mater. Charact. **107**, 79-84 (2015).

[27] H.Y. Song, H.T. Liu, H.H. Lu, L.Z. An, B.G. Zhang, W.Q. Liu, G.M. Cao, C.G. Li, Z.Y. Liu, G.D. Wang, Mater. Lett. **137**, 475-478 (2014).

[28] T. Kumano, T. Haratani, Y. Ushigami, ISIJ Int. **43** (5), 736-745 (2003).

[29] T. Kumano, T. Haratani, Y. Yshigami, ISIJ Int. **42** (4), 440-448 (2002).

[30] F.J. Humphreys, M. Hatherly, Recrystallization and Related Annealing Phenomena, Elsevier Science Ltd., Oxford (1995).

[31] F Shi, L.J. Wang, W.F. Cui, Y. Qi, C.M. Liu, T. Nonferr. Metal. Soc. **19**, 569-572 (2009).

[32] L.F. Fan, S.T. Qiu, L. Xiang, G.B. Tang, Mater. Trans. **55** (1), 123-127 (2014).

[33] J. Harase, R. Shimizu, J. Magn. Magn. Mater. **215**, 89-91 (2000).

[34] S. Nakashima, K. Takashima, J. Harase, ISIJ Int. **31** (9), 1013-1019 (1991).

[35] H.T. Liu, S.J. Yao, Y. Sun, F. Gao, H.Y. Song, G.H. Liu, L. Li, D.Q. Geng, Z.Y. Liu, G.D. Wang, Mater. Charact. **106**, 273-282 (2015).